

# Plug Conveying in a Vertical Tube

Martin Strauß<sup>a</sup> Sean McNamara<sup>a</sup> Hans J. Herrmann<sup>a</sup>  
 Gerhard Niederreiter<sup>b</sup> Karl Sommer<sup>b</sup>

<sup>a</sup>*Institut für Computerphysik, Universität Stuttgart, 70569 Stuttgart, GERMANY*

<sup>b</sup>*Lehrstuhl für Maschinen- und Apparatekunde, TU München, 85350 Freising,  
GERMANY*

## Abstract

Plug conveying along a vertical tube has been investigated through simulation, using a discrete element simulation approach for the granulate particles and a pressure field approach for the gas. The result is compared with an experiment. The dynamics of a plug are described by porosity, velocity and force profiles. Their dependence on simulation parameters provides an overall picture of plug conveying.

*Key words:* plug conveying, dense phase, pneumatic transport, granular medium  
*PACS:* 47.55.Kf, 45.70.Mg

## 1 Introduction

A quite common method for the transportation of granular media is pneumatic conveying, where grains are driven through pipes by air flow. Practical applications for pneumatic conveying can be found in food industry and in civil and chemical engineering. One distinguishes two modes of pneumatic conveying: dilute and dense phase conveying. Dilute phase conveying has been studied in much detail [1,2,3,4,5,6,7,8] and is well understood. The grains are dispersed and dragged individually by the gas flow and the interaction between grains is small. This is not true for the dense phase conveying, where the particle interaction is important and where particle density waves can be observed. Two modes of dense phase conveying can be distinguished, depending on the orientation of the pipe transporting the grains. In the horizontal transport the granular medium separates into two layers, the moving bed at the bottom of the pipe and the irregular transport by traveling dunes or slugs [9,10,11,12,13]. In the vertical transport the granular medium forms strands at medium gas velocities [14,15,16,17,18] and plugs at low gas velocities with high mass loads [19,20,12]; this mode is called plug conveying.

Currently plug conveying is gaining importance in industry, because it causes a lower product degradation and pipeline erosion than dilute phase conveying.

Unfortunately, current models [21,22] of plug conveying disagree even on the prediction of such basic quantities as the pressure drop and the total mass flow, and these quantities have a great impact in the industrial application. One of the reasons for the lack of valid models is that it is difficult to study plugs experimentally in a detailed way. Usually experimental setups are limited to the measurement of the local pressure drop, the total mass flux and the velocity of plugs. Most promising experimental studies have been performed by electrical capacity tomography [20,12] and stress detectors [23,24,13]. Simulational studies are handicapped by the high computational cost for solving the gas flow and the particle-particle interaction, and are therefore mostly limited to two dimensions. For the dense phase regime simulations have been done for bubbling fluidized beds [25,26,27,28,29,30], which show for high gas velocities first signs of pneumatic transport [31,32,33], for the strand type of conveying [16,15,18,34], and slugs in horizontal transport [9,35]. Simulations of vertical transport which show plugs with considerable length are rare. There is only one simulation of a short pipe in two dimensions by Tsuji et al. [19] and a picture of a single plug from a simulation with 50 particles in three dimensions by Ichiki et al. [36].

The goal of this paper is to provide a detailed view of plugs, by using a discrete element simulation combined with a solver for the pressure drop. This approach provides access to important parameters like the porosity and velocity of the granulate and the shear stress on the wall at relatively low computational cost. Contrary to the experiments, it is possible to access these parameters at high spatial resolution and without influencing the process of transportation at all. Additionally to plug profiles, characteristic curves of the pressure drop and the influence of simulation parameters are measured. The simulation results are compared with and verified by experiments.

## 2 Simulation Model

Plug conveying is a special case of the two phase flow of grains and gas. It is therefore necessary to calculate the motion of both phases, as well as the interaction between them. In the following, we explain how our algorithm treats each of these problems.

## 2.1 Gas Algorithm

The model for the gas simulation was first introduced by McNamara and Flekkøy [37] and has been implemented for the two dimensional case to simulate the rising of bubbles within a fluidized bed. For the simulation of plug conveying we developed a three dimensional version of this algorithm.

The algorithm is based on the mass conservation of the gas and the granular medium. Conservation of grains implies that the density  $\rho_p$  of the granular medium obeys

$$\frac{\partial \rho_p}{\partial t} + \vec{\nabla} \cdot (\vec{u} \rho_p) = 0, \quad \rho_p = \rho_s(1 - \phi), \quad (1)$$

where the specific density of the particle material is  $\rho_s$ , the porosity of the medium is  $\phi$  (i.e. the fraction of the space available to the gas), and the velocity of the granulate is  $\vec{u}$ .

The mass conservation equation for the gas is

$$\frac{\partial \rho_g}{\partial t} + \vec{\nabla} \cdot (\vec{v}_g \rho_g) = 0, \quad \rho_g \propto \phi P, \quad (2)$$

where  $\rho_g$  is the density of the gas and  $\vec{v}_g$  its velocity. This equation can be transformed into a differential equation for the gas pressure  $P$  using the ideal gas equation, together with the assumption of uniform temperature.

The velocity  $\vec{v}_g$  of the gas is related to the granulate velocity  $\vec{u}$  through the d'Arcy relation:

$$-\vec{\nabla} P = \frac{\eta}{\kappa(\phi)} \phi (\vec{v}_g - \vec{u}), \quad (3)$$

where  $\eta$  is the dynamic viscosity of the air and  $\kappa$  is the permeability of the granular medium. This relation was first given by d'Arcy in 1856 [38]. For the permeability  $\kappa$  the Carman-Kozeny relation [39] was chosen, which provides a relation between the porosity  $\phi$ , the particle diameter  $d$  and the permeability of a granular medium of monodisperse spheres,

$$\kappa(\phi) = \frac{d^2 \phi^3}{180(1 - \phi)^2}. \quad (4)$$

After linearizing around the normal atmospheric pressure  $P_0$  the resulting differential equation only depends on the relative pressure  $P'$  ( $P = P_0 + P'$ ), the porosity  $\phi$  and the granular velocity  $\vec{u}$ , which can be derived from the particle simulation, and some constants like the viscosity  $\eta$ :

$$\frac{\partial P'}{\partial t} = \frac{P_0}{\eta \phi} \vec{\nabla} (\kappa(\phi) \vec{\nabla} P') - \frac{P_0}{\phi} \vec{\nabla} \vec{u}. \quad (5)$$

This differential equation can be interpreted as a diffusion equation with a diffusion constant  $D = \phi\kappa(\phi)/\eta$ . The equation is solved numerically, using a Crank-Nickelson approach for the discretization. Each dimension is integrated separately.

The boundary conditions are imposed by adding a term  $\mp S$  on the right hand side of equation (5) at the top and the bottom of the tube, where  $S \propto v_g P_0$ . This resembles a constant gas flux with velocity  $v_g$  at a pressure  $P_0$  into and out of the tube.

## 2.2 Granulate Algorithm

The model for the granular medium simulates each grain individually using a discrete element simulation (DES). For the implementation of the discrete element simulation we used a version of the molecular dynamics method described by Cundall [40]. The particles are approximated as monodisperse spheres, rotations in three dimensions are taken into account.

The equation of motion for an individual particle is

$$m\ddot{\vec{x}} = m\vec{g} + \vec{F}_c - \frac{\vec{\nabla}P}{\rho_s(1-\phi)}, \quad (6)$$

where  $m$  is the mass of a particle,  $\vec{g}$  the gravitation constant and  $\vec{F}_c$  the sum over all contact forces. The last term, the drag force, is assumed to be a volume force given by the pressure drop  $\vec{\nabla}P$  and the local mass density of the granular medium  $\rho_s(1-\phi)$ .

The interaction between two particles in contact is given by two force components: a normal and a tangential component with respect to the particle surface. The normal force is the sum of a repulsive elastic force (Hooke's law) and a viscous damping. The tangential force is proportional to the normal force (sliding Coulomb friction) or a viscous damping. The viscous damping is used when the relative surface velocity of the particles in contact is small. The same force laws are considered for the interaction between particles and the tube wall.

## 2.3 Gas-Grain Interaction

The simulation method uses both a continuum and a discrete element approach. While the gas algorithm uses fields, which are discretized on a cubic grid, the granulate algorithm describes particles in a continuum. A mapping

is needed for the algorithms to interact. For the mapping a tent function  $F(\vec{x})$  is used:

$$F(\vec{x}) = f(x)f(y)f(z), \quad f(x) = \begin{cases} 1 - |x/l|, & |x/l| \leq 1, \\ 0, & 1 < |x/l|, \end{cases} \quad (7)$$

where  $l$  is the grid constant used for the discretization of the gas simulation.

For the gas algorithm the porosity  $\phi_j$  and the granular velocity  $\vec{u}_j$  must be derived from the particle positions  $x_i$  and velocities  $v_i$ , where  $i$  is the index of particle and  $j$  is the index for the grid node. The tent function distributes the particle properties around the particle position smoothly on the grid:

$$\phi_j = 1 - \sum_i F(\vec{x}_i - \vec{x}_j), \quad \vec{u}_j = \frac{1}{1 - \phi_j} \sum_i \vec{v}_i F(\vec{x}_i - \vec{x}_j), \quad (8)$$

where  $x_j$  is the position of the grid point and the sum is taken over all particles.

For the computation of the drag force on a particle the pressure drop  $\vec{\nabla}P_i$  and the porosity  $\phi_i$  at the position of the particle are needed. These can be obtained by a linear interpolation of the fields  $\vec{\nabla}P_j$  and  $\phi_j$  from the gas algorithm:

$$\phi_i = \sum_j \phi_j F(\vec{x}_j - \vec{x}_i), \quad \vec{\nabla}P_i = \sum_j \vec{\nabla}P_j F(\vec{x}_j - \vec{x}_i), \quad (9)$$

where the sum is taken over all grid points.

### 3 Experimental Results

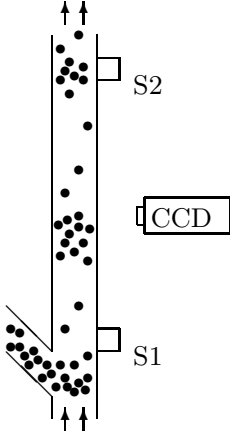


Fig. 1. Sketch of the experimental setup. Gas is inserted at a constant mass rate at the bottom of the tube, the granulate enters from the left. S1 and S2 denotes pressure sensors. A CCD camera is used to record the transport at mid-height.

In the experiment we study the vertical pneumatic transport of wax beads of diameter  $d = 1.41\text{mm}$ , density  $\rho_s = 937\text{kg/m}^3$  and a Coulomb coefficient of 0.21. The experimental transport channel is a vertical tube (PMMA) of length  $l = 1.01\text{m}$  and of internal diameter  $D_t = 7\text{mm}$ . These parameters were chosen to be able to compare to simulations with little computational effort possible. The air is injected at a constant mass flow rate at the bottom of the tube. The granular medium is injected from the side from a tube with a slope of  $45^\circ$ .

The wax beads, when leaving the vertical tube at the top, are gathered and weighted. From this data the mass flow rate of the granular medium can be obtained. The total pressure drop is detected through two pressure sensors, one at the bottom (S1) and one at the top (S2). The velocity and length of the plugs can be obtained by a CCD-camera (30 frames per second) positioned at the middle of the tube.

series		A	B	C
air flow	( $\text{l/min}$ )	2.0	2.2	2.4
pressure drop	( $\text{hPa/m}$ )	$42 \pm 2$	$45 \pm 2$	$44.5 \pm 2$
granulate flow	( $\text{kg/h}$ )	$1.7 \pm 0.15$	$2.49 \pm 0.02$	$2.88 \pm 0.08$
plug velocity	( $\text{m/s}$ )	0.09-0.17	0.12-0.19	0.18-0.33
plug length	( $\text{cm}$ )	0.6-4	1.7-9	0.5-4

Table 1

Experimental results for vertical plug conveying in a tube of length  $l = 1.01\text{ m}$  and diameter  $D_t = 7\text{ mm}$  using wax beads ( $d = 1.4\text{ mm}$ ) as granular medium.

Plug conveying is observed, as shown in figure 2. The range of parameters

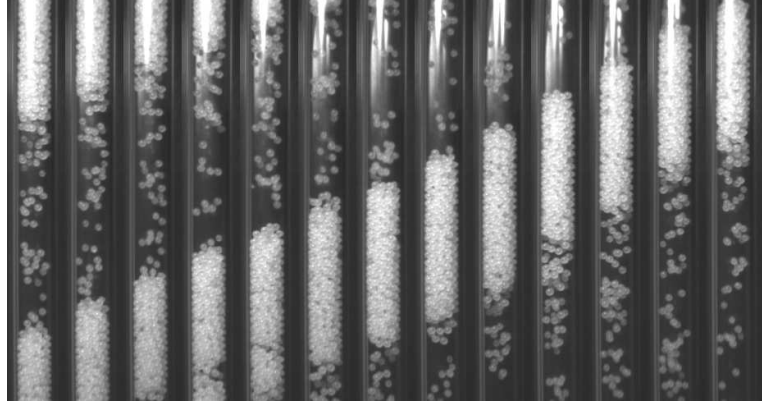


Fig. 2. A series of photos showing a plug moving upwards. The height of the shown tube is 9 cm, the frame rate is 30 Hz, from measurement series B.

for plug conveying in the experiment were rather limited. The plugs often get stuck in the tube, interrupting the plug transport completely. For long runs and repeated use of grains, electrostatic forces influenced the results. Measurement series for three different air flow rates were made. The results for the total pressure drop and the granular flow are given in table 1, for more details see [41].

## 4 Simulational Results

The setup for the simulation is almost the same as for the experiment. The main difference is: particles are injected from the bottom at a constant mass flow rate. As default the mass flow rate of the granular medium is chosen equal to the measured flow rate in the experiment ( $2.49 \text{ kg/h}$ ). Default parameters for the particles are: diameter  $d = 1.4 \text{ mm}$ , density  $\rho_s = 937 \text{ kg/m}^3$ , Coulomb coefficient  $\mu = 0.5$  and restitution coefficient  $e = 0.5$ . Simulations are preformed for half tube length  $L_t = 0.525 \text{ m}$  and tube diameter  $D_t = 7 \text{ mm}$ . The resulting gas volume has been discretized into  $150 \times 2 \times 2$  grid nodes, which corresponds to a grid constant of  $3.5 \text{ cm}$ . The gas pressure is set to  $P_0 = 1013.25 \text{ hPa}$ . Simulations are preformed for gas viscosities  $\eta$  from  $0.045 \text{ cP}$  to  $0.085 \text{ cP}$  and gas flows  $\dot{V}$  between  $1.1 \text{ l/min}$  and  $9.2 \text{ l/min}$ . The gas flow is usually given as the superficial gas velocity  $v_s = \phi v_g = 4\dot{V}/\pi D_t^2$  [42], which is the equivalent gas velocity for an empty tube.

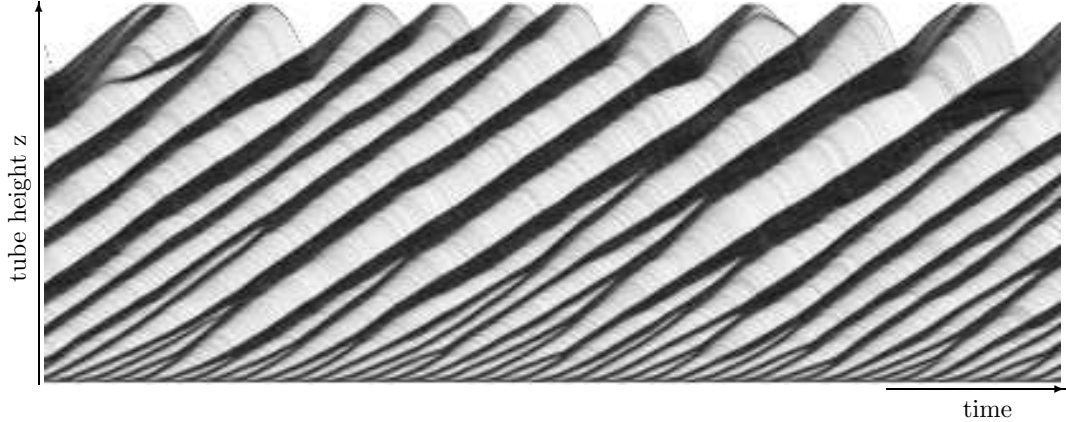


Fig. 3. Spatio-temporal image of the porosity along the vertical tube. The dark regions correspond to low porosity, light regions to high porosity. The entire tube ( $52.5 \text{ cm}$ ) is displayed, the elapsed time is  $4 \text{ s}$ . Default parameters for the simulation were used, the superficial gas velocity is  $1 \text{ m/s}$ , the gas viscosity is  $0.0673 \text{ cP}$ , the Coulomb coefficient is  $0.5$ . Particles are introduced at the bottom and on average 3600 particles are within the tube at a pressure drop of  $39 \text{ hPa/m}$ .

The flow in the experiment is turbulent (particle  $Re \approx 65$ ). In the simulation, an effective gas viscosity is used to account for the turbulence. For an effective gas viscosity  $\eta = 0.0673 \text{ cP}$ , a gas flow  $\dot{V} = 2.3 \text{ l/min}$  and a Coulomb coefficient  $\mu = 0.5$  plug conveying is observed as shown in figure 3. The observed pressure drop  $39 \text{ hPa/m}$ , the plug velocity  $0.24 \text{ m/s}$  and the plug length  $2\text{-}4 \text{ cm}$  fit well with the experimental results.

As pointed out in the introduction, only very limited simulations of vertical plug conveying have been published. Vertical transport has been studied by Tsuji [19], but his simulation was limited to a short pipe in two dimensions ( $L_t \approx 3d$ ). In his case the tube contained about 300 particles, which is in our

case about the number of particles within one plug. Three dimensional plugs of about 50 particles have also been found by Ichiki [36], but no analysis of them was done. Thus our simulations are the first to show full featured vertical plug conveying at the level of grains in three dimensions.

#### 4.1 Characteristic curves

The “characteristic curves” of a pneumatic transport system are plots of the pressure drop against the superficial gas velocity  $v_s = \phi v_g$  for different mass flows of the granulate. This kind of diagram is highly dependent on the material characteristics of the tube wall and the granulate and can be used to predict the overall transport performance for given parameter sets. Such a diagram, from data from our simulation, is shown in figure 4.

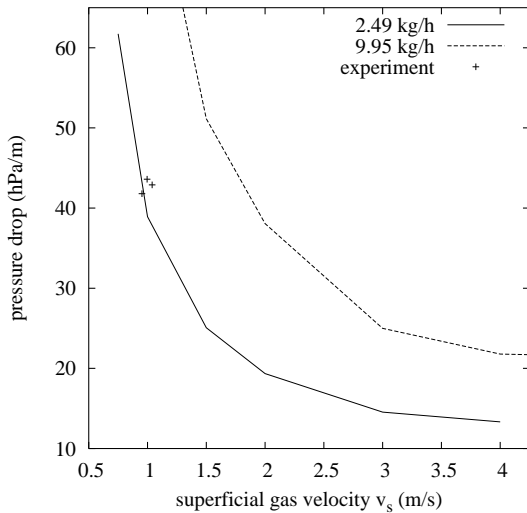


Fig. 4. Total pressure drop against superficial gas velocity for different granular mass flows. Plotted are characteristic curves from the simulation for the granular mass flows  $2.49\text{ kg}/\text{h}$  and  $9.95\text{ kg}/\text{h}$ , and the three data points from the experiment with granular mass flows  $1.7 - 2.9\text{ kg}/\text{h}$ . For mass flow  $2.49\text{ kg}/\text{h}$  plugs stick when the superficial gas velocity is below  $0.75\text{ m}/\text{s}$ .

The diagram provides the typical qualitative behavior for pneumatic transport. From top left to bottom right with increasing superficial gas velocity, four regions can be distinguished. First, for small superficial gas velocities ( $v_s < 0.5\text{ m}/\text{s}$ ), there is bulk transport. The tube is completely filled with granulate, so the pressure drop is high. Nevertheless the drag force on the bulk is too small to support the weight of the granular medium. In this case the transport comes through the enforced granular mass flow at the bottom.

For slightly higher gas velocities ( $0.5\text{ m}/\text{s} \leq v_s < 0.75\text{ m}/\text{s}$ ) the first plugs appear. These plugs are often not able to compensate the force from material



Fig. 5. Spatio-temporal image of the porosity along the vertical tube. The dark regions correspond to low porosity, light regions to high porosity. The entire tube ( $52.5\text{ cm}$ ) is displayed, the elapsed time is  $4\text{ s}$ . A lower superficial gas velocity ( $0.75\text{ m/s}$ ) has been used than in figure 3. On average 4900 particles are within the tube at a pressure drop of  $62\text{ hPa/m}$ . Due to the low drag force the plugs quickly coalesce into very long plugs.

falling onto them. They usually collapse into big plugs sticking in the tube or their motion is reduced considerably (fig. 5). In this region the pressure drop decreases rapidly with increasing gas velocity.

For moderate velocities plug conveying is observed  $0.75\text{ m/s} \leq v_s < 4\text{ m/s}$  (fig. 3). The qualitative behavior of the granular medium in this regime is the same in the experiment and the simulation. The particles injected at the bottom organize into plugs. After a short acceleration at the bottom plugs move upwards with a constant velocity. When two plugs collide, they combine into a single plug. A plug always loses particles at the bottom and usually maintains its length by collecting particles at the top. A plug disintegrates when it gets too small. The porosity of the granular medium within a plug is close to the minimum porosity, the edges are sharp and the space between plugs is rather empty ( $\phi > 90\%$ ). As one can see in figure 4 the experimental data were measured for a superficial gas velocity at the lower limit for plug conveying. In this region the pressure drop is highly dependent on the material parameters ( $\eta, P_0, \mu$ ).

For high superficial gas velocities ( $v_s > 4\text{ m/s}$ ) the tube is almost empty (fig. 6), in the simulation the particles are pushed out as small plugs. Their porosity increases with the superficial gas velocity. In this region the simulation method underestimates the pressure drop, because it does not consider the increasing drag force on single particles, which in the experiment dominates in this region. The regions as described above shift with changes of the simulation parameters.

A nearly proportional relation is observed between the total pressure drop



Fig. 6. Spatio-temporal image of the porosity along the vertical tube. The dark regions correspond to low porosity, light regions to high porosity. The entire tube ( $52.5\text{ cm}$ ) is displayed, the elapsed time is  $4\text{ s}$ . A higher superficial gas velocity ( $4\text{ m/s}$ ) has been used compared to the spatio-temporal image in figure 3 ( $1\text{ m/s}$ ). On average 850 particles are within the tube at a pressure drop of  $13\text{ hPa/m}$ .

and the total number of particles in the tube. This can be explained by the observation that the amount of particles between the plugs is small and most particles are densely packed at a well defined porosity in the plugs. Through the d'Arcy's law, the total pressure drop depends linearly on the tube length filled with this porosity. The pressure drop on the granulate between the plugs is negligible and causes only a small deviation from the proportional relation. At high gas velocities this is no longer true, because there is no dominating porosity for the plugs.

In the following the dependence of the pressure drop on the air viscosity  $\eta$ , the atmospheric pressure  $P_0$  and the Coulomb coefficient  $\mu$  is discussed. For the parameter studies the superficial gas velocity has been fixed to  $1\text{ m/s}$ . This resembles the gas velocities used for the experiment. For higher velocities the parameter dependence decreases.

The gas algorithm can be influenced by changing the atmospheric pressure  $P_0$  or the diffusion constant  $D$ . An increase in background pressure  $P_0$  combined with a proportional increase in superficial velocity leaves the pressure drop unchanged. This can be deduced directly from equation (5) by noting that both terms on the right hand side are proportional to  $P_0$ .

The diffusion constant  $D \propto d^2/\eta$  can be changed through the particle diameter  $d$  and the viscosity  $\eta$ . Therefore it is sufficient to analyze the parameter space for the viscosity at a constant diameter as shown in figure 7.

The viscosity dependence of the pressure drop can be described by a hyperbola. The pressure drop converges for high viscosities to a finite value. In this case the pressure drop supports the weight of the granulate embedded in the fluid

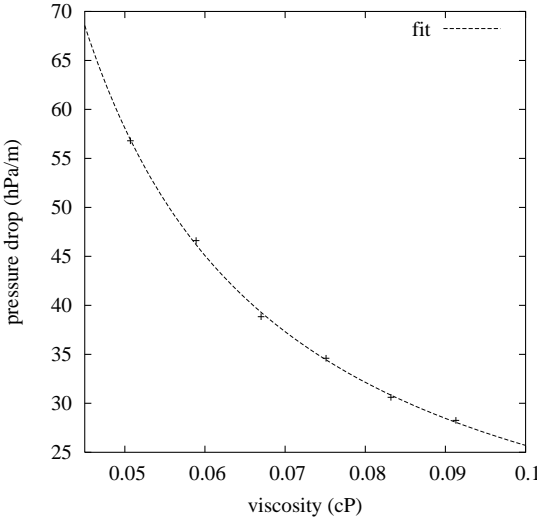


Fig. 7. Dependence of the pressure drop on the dynamic viscosity  $\eta$  of the gas at superficial gas velocity  $1\text{ m/s}$ . The data points can be fitted by a hyperbola.

and depends only on the velocity of the gas and the enforced mass flow of the granular medium. For small viscosities plug conveying starts to break down to bulk transport. The pressure drop diverges at the viscosity where the drag force can no longer balance the weight and friction of the bulk.

The parameter of the particle simulation with most influence on the transport of the granular medium is the Coulomb coefficient, i.e. an increase of the restitution coefficient from  $e = 0.5$  to  $e = 0.99$  leaves the pressure drop unchanged. As one can see in figure 8 the pressure drop increases with raising Coulomb

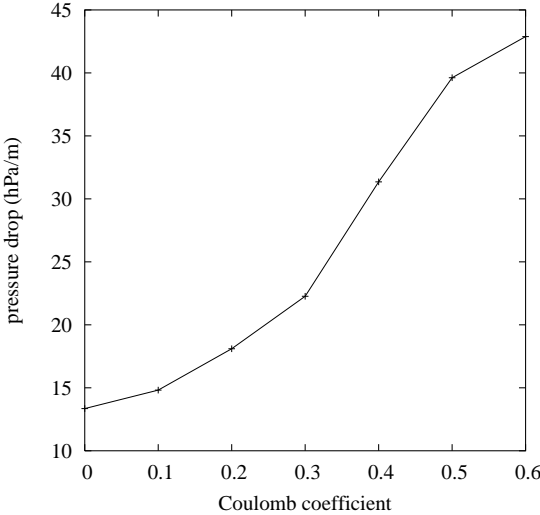


Fig. 8. Dependence of the pressure drop on the Coulomb coefficient, the superficial gas velocity is  $1\text{ m/s}$ . For high Coulomb coefficient ( $\mu > 0.5$ ) a transition from plug conveying to bulk transport can be observed.

coefficients. For low coefficients,  $0 < \mu \leq 0.5$ , plug conveying is observed,

for higher Coulomb coefficients the plugs get sticky and coalesces into a big, slowly moving plug. These plugs are similar to the ones for low superficial gas velocities (fig. 5).

#### 4.2 Plug statistics

The spatio-temporal image of the porosity along the vertical tube (fig. 3) provides a rough picture of plugs and their movement along the tube. A statistical approach is necessary to get more precise values. Properties of interest are the porosity and the granular velocity within a plug, the plug length, and their dependence on the vertical position  $z$  of the plug within the tube. To get some average values for the porosity and the granular velocity, the tube was segmented into horizontal slices of height 3.5 mm. For each slice the average porosity and granular velocity has been computed every 0.01 s. The contribution of a particle has been weighed by the volume occupied by that particle within a given slice.

The resulting vertical porosity has been used to identify plugs. Every region with a porosity lower than 0.6 is defined to belong to a plug.

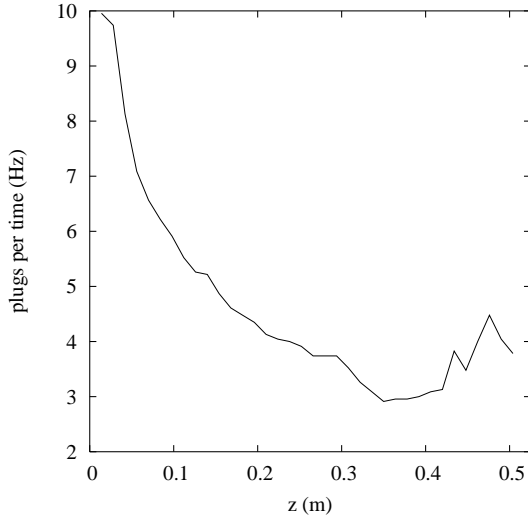


Fig. 9. Number of plugs per time as a function of height  $z$ . The corresponding spatio-temporal image is shown in figure 3. The total tube height is 52.5 cm, default parameters are used. The data is averaged over 23 s.

Figure 9 shows the number of plugs per time as a function of height. At the bottom of the tube the incoming granular medium forms into a lot of small plugs. Even though their velocity is low, the resulting plug rate is high. As can be seen in figure 3, plugs collide along the tube and merge into bigger plugs. The merging of plugs reduces the plug rate along the tube. The smooth

decrease of the plug rate indicates that there is no preferred height for the collision and merging of plugs.

For each plug the center of mass, the minimal porosity, the maximal granular velocity and the plug length have been computed.

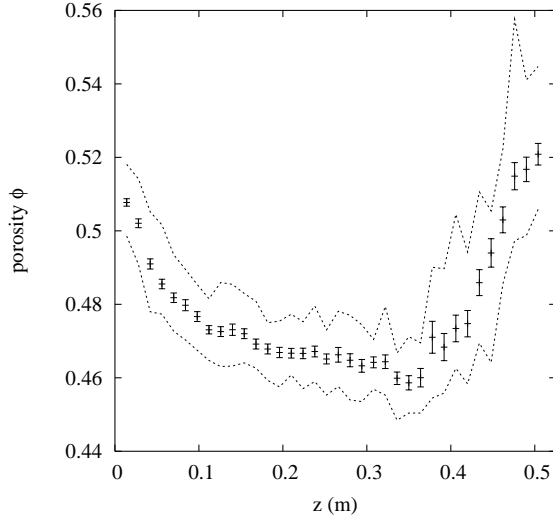


Fig. 10. Minimal porosity found in plugs at height  $z$ , corresponding to the plug rate shown in figure 9. The bars denote the uncertainty of the average, and the dotted lines indicate the width of the distribution; at each value of  $z$ , half of the observed plugs have a porosity lying between the upper and the lower dotted lines. The plug porosity decreases at the bottom when the granulate enters the tube ( $z < 0.1\text{ m}$ ) and increases at the top of the tube ( $z > 0.4\text{ m}$ ), when the preceding plug has been removed.

Figure 10 shows the minimum plug porosity as a function of the vertical position  $z$  of a plug. At each value of  $z$ , the mean porosity and its uncertainty (standard deviation divided by the square root of the number of plugs) were calculated. These quantities are shown by the bars in Figure 10. To show the distribution of porosity about the mean, the two dotted lines were added. At each height  $z$ , half of the plugs have a porosity lying between these two lines. The same analysis was carried out for the data in Figures 11 and 12. As one can see in figure 10 at the left of the graph, the granular medium is inserted at the bottom of the tube with a porosity of 0.51. From there the porosity decreases quickly to about 0.47 at a height  $z = 0.1\text{ m}$  and then remains almost constant until  $z = 0.3\text{ m}$ . At the top of the tube ( $z > 0.3\text{ m}$ ) the porosity increases until the grains leave the simulation space at  $z = 0.525\text{ m}$ .

Figure 11 shows the corresponding particle velocity. The change in porosity comes along with an increase of the granular velocity within the plugs. The granulate is inserted at the bottom with an initial velocity of  $0.04\text{ m/s}$ . The granular velocity saturates to a final velocity for the granular velocity at a height of  $0.1\text{ m}$ . At a height of about  $0.35\text{ m}$  the granular medium accelerates

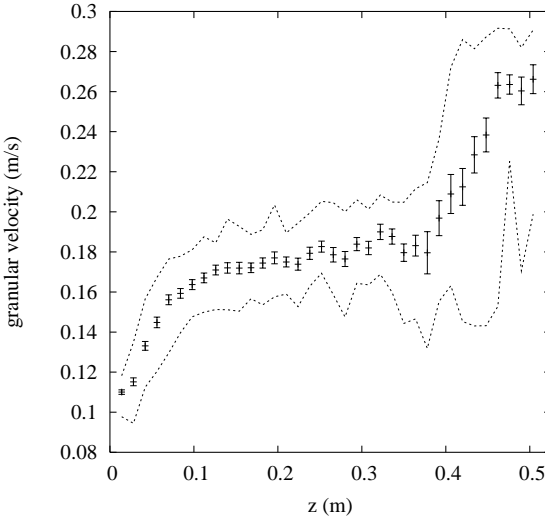


Fig. 11. Maximal granular velocity found in plugs at height  $z$ , corresponding to the plug rate shown in figure 9. The bars and dotted lines have the same meaning as in figure 10. The granular velocity saturates in the middle of the tube, the increase of the granular velocity at the bottom and at the top of the tube is due to the boundary effects described in figure 10.

until the grains leave the tube.

An explanation for the final constant plug velocity can be derived using the balance equation for the forces on a plug:

$$F = -mg - F_c + \alpha(\phi)(v_g - u). \quad (10)$$

where  $m$  is the mass of a plug,  $g$  is the gravity constant,  $F_c$  is the force on the plug through the friction with the wall and the collisions of particles falling onto the plug. The last term  $\alpha(\phi)(v_g - u)$  is the drag force on the plug, which is proportional to the relative velocity between the particles and the gas within the plug. At the middle of the tube the porosity of the plug  $\phi$  is constant. On small time scales the mass  $m$  and the gas velocity  $v_g$  can be assumed constant. Only the drag force depends on the granular velocity  $u$  through d'Arcy's law. For a certain granular velocity the drag force balances the sum of gravitational and friction forces. If there is no acceleration of the plug, then  $u$  remains constant. The solution is stable under small fluctuations in  $u$ .

Figure 12 shows the mean plug length along the tube. The average plug length is increasing along the tube, due to merging of plugs. Unlike the previous cases no equilibrium length is found. The increase of the plug length combined with the decrease of the number of plugs per time (fig. 9) conserves the mass flux of the granulate.

As can be seen in figure 3, the change in porosity, velocity and plug length at the top of the tube can be explained by the lack of grains falling onto the top

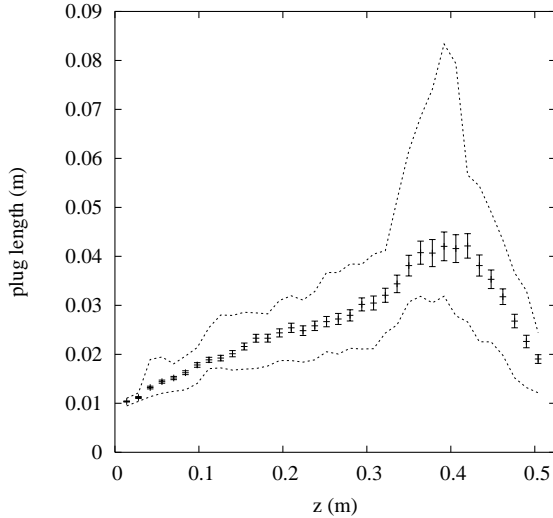


Fig. 12. Mean plug length at tube height  $z$ , corresponding to the plug rate shown in figure 9. The bars and dotted lines have the same meaning as in figure 10. The average plug length increases along the tube, consistent with the decrease in the plug rate (fig. 9).

of the uppermost plug.

The diagrams in figures 10 to 12 imply, that there is a typical porosity, granular velocity and length of plugs for a given height and a characteristic plug profile exists. In the following averaged vertical and radial profiles of plugs at the height of  $0.26\text{ m}$  are discussed. To get some sensible profiles the plugs were selected with length and granular velocity close to the mean values ( $L_t = 0.024 \pm 0.01\text{ m}$ ,  $u = 0.16 \pm 0.02\text{ m/s}$ ).

### 4.3 Vertical plug profiles

While in experiments recognizing and measuring parameters for global plug conveying are rather simple, the measurement of profiles for individual plugs remains a nearly impossible task. So one of the reasons for simulating plug conveying is to provide a detailed picture of what happens within a plug, and how parameters like porosity, granular velocity or shear stress change along the plug.

A porosity profile of an averaged plug is shown in Figure 13. The provided profiles (fig. 13-19) average over seven plugs. These plugs were taken from the middle of the tube  $z = 0.26\text{ m}$  with granular velocity  $0.16 \pm 0.02\text{ m/s}$  and plug length  $0.024 \pm 0.01\text{ m}$ . The coordinate  $\Delta z$  denotes the relative vertical position along the tube with respect to the center of mass. At the top of the

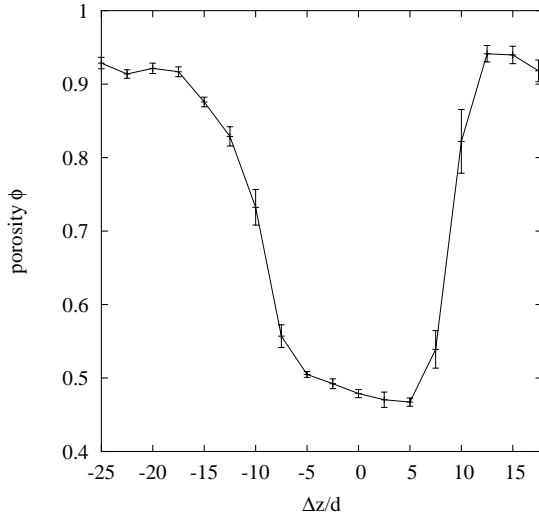


Fig. 13. Vertical porosity profile along an averaged plug, containing about 320 particles, positioned at the middle of the tube. The profile was averaged over seven plugs with granular velocity  $0.16 \pm 0.02\text{ m/s}$  and plug length  $0.024 \pm 0.01\text{ m}$ . The data belong to the simulation displayed in figure 3. The horizontal axis denotes the relative vertical position  $\Delta z$  along the tube with respect to the center of mass. The vertical position is given in multiples of the particle diameter  $d = 1.4\text{ mm}$ .

plug, on the right hand side of figure 13, the porosity decreases quickly from 90% to 45%. In the middle the porosity of the plug remains almost constant, and increases slowly at the bottom. The minimum porosity is bigger than a random dense packing due to near wall effects.

Figure 14 displays the velocity profile of the granular medium in the region of the plug shown in Figure 13. One can distinguish four different regions: Above the plug ( $15 \leq \Delta z/d$ ) the granulate particles are falling downwards, the porosity is high. These particles originate from the bottom of an upper

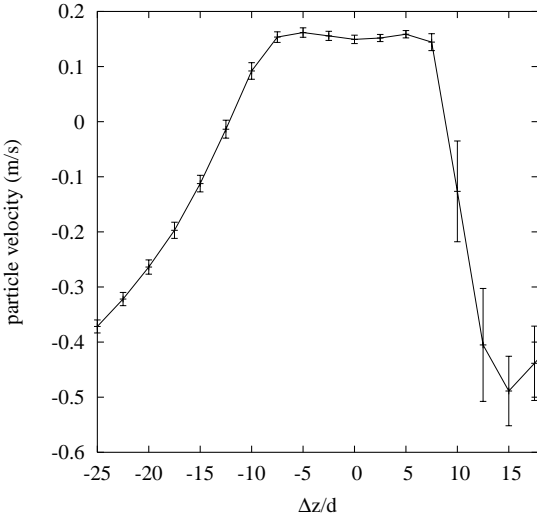


Fig. 14. Velocity of the granular medium along the averaged plug of figure 13. Inside the plug ( $|\Delta z/d| > 7$ ) the velocity is constant, outside the granular medium accelerates downwards.

plug. The drag force cannot support their weight due to the high porosity. At the top of the plug the particles collide with the low porosity region and decelerate rapidly ( $7 < \Delta z/d \leq 15$ ). The granular medium gets denser as particles are added to the plug. In the following, this region at the top of the plug will be called collision region. Inside the plug, where the porosity settles to a low value, the granulate velocity is almost constant ( $|\Delta z/d| > 7$ ). At the bottom ( $-10 < \Delta z/d \leq -7$ ) of the plug the granular medium starts to accelerate downwards again. Thus the plug is always loosing material at the bottom. This region will be called disintegration region.

The trajectory of a single particle through the plug can be sketched by a snapshot of the vertical forces within a plug. Figure 15 displays the drag force  $F_d$  and the sum over the interparticle, gravity and friction forces on a particle (here called particle forces)  $F_p$ . These forces are averaged over the horizontal plane. Above the plug, the particle accelerates constantly due to gravity. The drag force on a single particle can be neglected, as the particle velocity is far from the terminal velocity. The high peak in the particle force marks the collision region. The huge fluctuations in the particle force arise, when the falling particle collides with the top of the plug front. Within the collision region the porosity decreases and therefore the drag force increases. Below the collision region, within the plug, the drag force and the particle force balance each other. At the bottom of the plug the friction force drops to zero and gravity and drag force are in equilibrium. Below this point the disintegration region begins, the granular velocity within the plug decreases, the porosity increases. After a short distance the drag force is zero and the particles are falling freely again.

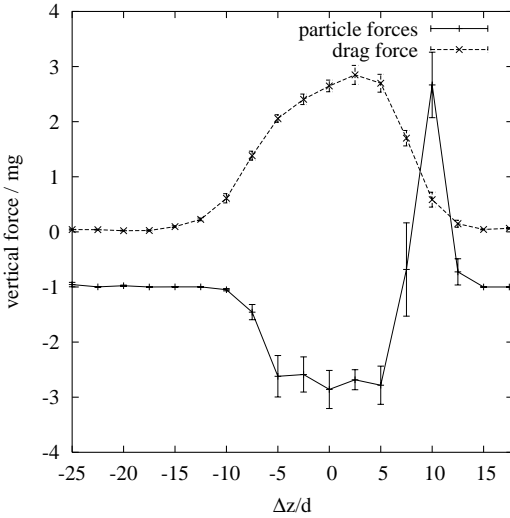


Fig. 15. Forces acting on particles along the averaged plug in figure 13. Interparticle forces, gravity and friction are summed up and displayed as particle force. The drag force corresponds to the pressure drop of the gas. Outside of the plug ( $|\Delta z/d| > 15$ ) the particle force is  $mg$ , indicating that the particle are freely falling. The peak in the particle force corresponds to the collision region, where particles fall onto the plug.

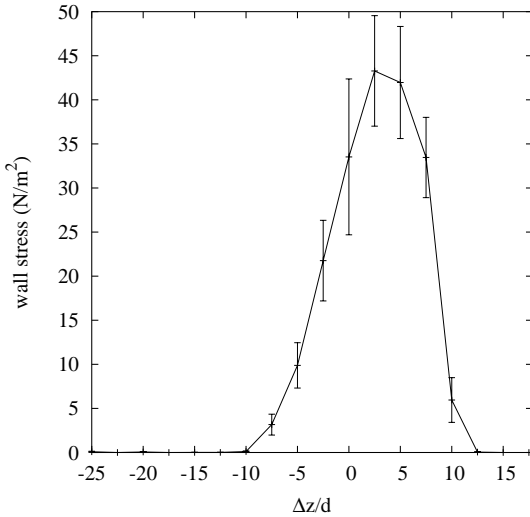


Fig. 16. Stress between the wall and the granular medium along the averaged plug in figure 13. The wall stress is limited to the plug, where the porosity is low (< 70%).

The normal wall stress corresponding to the plug in Figure 13 is shown in Figure 16. Due to the implementation of the simulation and the high damping the normal wall stress is proportional to the vertical shear stress (Coulomb friction). The wall stress is limited to the plug including the collision and disintegration region. The wall stress increases from zero within the collision region and then slowly decreases, reaching zero in the disintegration region. The maximal wall stress is of the same order of magnitude as the

pressure imposed on the plug front by the falling granulate  $P = \rho_s(1 - \phi)v^2 = 937 \text{ kg/m}^3 \cdot 0.07 \cdot (0.7 \text{ m/s})^2 \approx 32 \text{ Pa}$ .

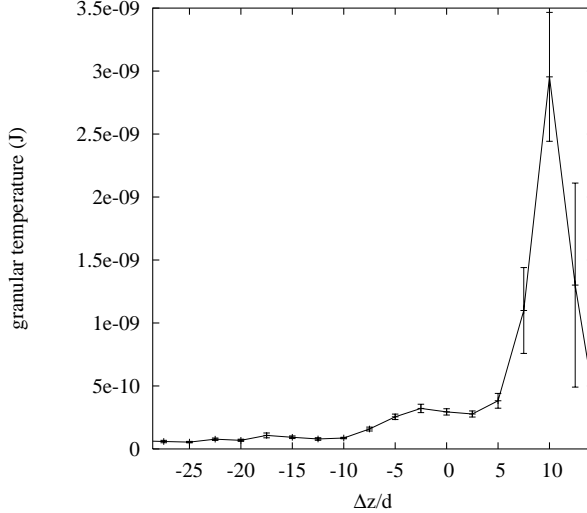


Fig. 17. Granular temperature along the averaged plug in figure 13. The granular temperature is only non-zero near the collision region between the plug and the falling particles at the top of the plug. Due to the large damping ( $e = 0.5$ ) the granular temperature is dissipated quickly and remains on a low level within the plug ( $|\Delta z/d| > 7$ ).

Figure 17 shows the granular temperature along a plug. The granular temperature is the average kinetic energy of particles minus the kinetic energy of the motion of their center of mass. Appreciable granular temperatures occur in the collision region. Due to the high damping ( $e = 0.5$ ) these temperatures are confined to a small region at the top front of the plug. There is a finite granular temperature within the plug, the temperature drops nearly to zero at the bottom of the plug.

#### 4.4 Radial plug profiles

Another point of view on the plug is given by the radial profiles. The volume used for averaging at a given radius is a cylindrical ring with a height of 1.5 particle diameters and a width of 0.25 particle diameters. The porosity at a given range is defined to be the volume fraction of the gas within the cylindrical ring.

As a result of this high radial resolution it is possible to resolve layers of granular particles. As can be seen in figure 18, the plugs, averaged for the vertical profiles, are highly ordered in the radial direction. The radial profiles are taken from the middle of the averaged plugs, at half height of the tube ( $z = 0.26 \text{ m}$ ). The porosity minima in figure 18 correspond to three layers

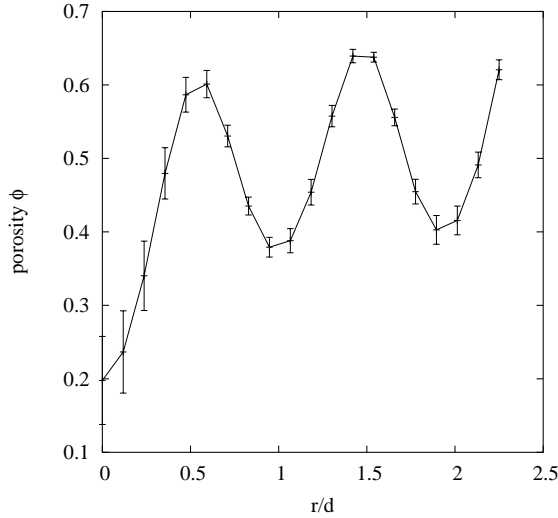


Fig. 18. Radial porosity profile through an averaged plug at the height  $z = 0.26\text{ m}$ . The same plugs were used for averaging as for the vertical profiles in figure 13. The radial distance  $r$  from the middle of the tube is given in units of the particle diameter  $d = 1.4\text{ mm}$ . The porosity minima correspond to three layers of particles moving upwards, parallel to the tube wall.

of particles. This agrees well with the ratio between the tube and particle diameter, which implies that five particles fit into the tube horizontally. The minimum at  $r/d = 0$  corresponds to a vertical string of particles in the middle of the tube, the layer at  $r/d = 2$  touches the wall of the tube. For higher radii  $r$  the porosity increases to one. The large error at the center of the tube is due to the smaller volume involved for averaging.

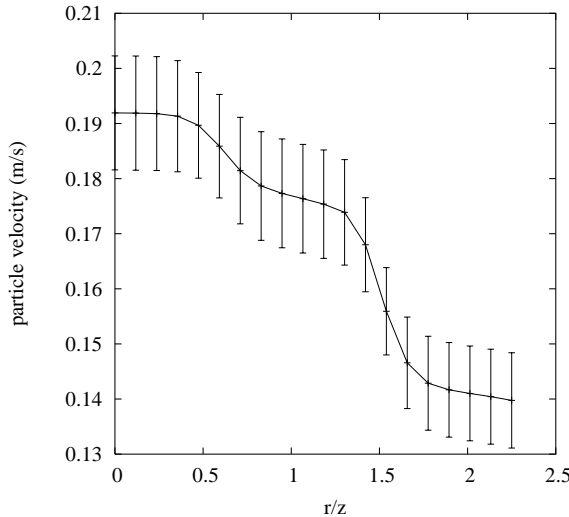


Fig. 19. Radial profile of the granular velocity for an averaged plug in figure 18. The profile shows three layers of particles moving upwards with different velocities. The layer along the wall is the slowest due to the friction with the wall.

The radial profile of the granular velocity (fig. 19) shows that the layers ob-

served in the porosity profile move with different velocities. The layer at the wall, which has the largest impact on the total averaged granular velocity, moves slowest, due to the friction with the wall.

## 5 Conclusion

In this paper a simple model [37] with coupled grain and gas flow has been applied to pneumatic transport. The implementation is three-dimensional; rotation and Coulomb friction are taken into account. The flux of gas and grains is set by the boundary conditions. Plug conveying is observed. The simulation used for plug statistics and profiles contained on average 3600 particles in a tube of length  $0.525\text{ m}$  and diameter  $7\text{ mm}$ . The simulation lasted  $23\text{ s}$ ; during this time 90 different plugs were observed at the middle of tube, each with about 300 particles. Additionally 24 simulations were preformed to obtain the characteristic curves.

The behavior of the granular medium and the gas is consistent with experimental observations. The pressure drop, mass flux and superficial velocity can be obtained in quantitative agreement with experiment by introducing an effective viscosity  $\eta$  and an effective friction  $\mu$ . The effective viscosity reflects the increased momentum transport in the gas due to the turbulent flow around the grains. The effective friction reflects the complex interplay between sliding, rolling and static friction. By using the model, large numbers of plugs could be studied, and their porosity, velocity, and size were measured as functions of height.

The simulation results imply that the formation of the plugs at the bottom of the tube occurs spontaneously. There is a well defined preferred velocity of the plugs, which is independent of the plug size and the tube length. The average plug length increases along the tube due to the merging of plugs. To confirm experimentally the constant velocity and the increase of plug length, statistics of plug length and velocity at different heights along the tube are needed. The results also show that boundary effects at the bottom and the top of the tube have to be taken into account. For the experimental parameters the influence of the boundaries is limited to a distance of  $0.1\text{ m}$ , which is about the distance between two plugs in the middle of the tube. Plugs accelerate in these boundary regions. The acceleration at the upper boundary arises due to the lack of grains falling on the uppermost plug. This implies that the momentum transfer due to falling grains can not be neglected. A model of plug conveying must take into account that these falling grains reduce the plug velocity.

Also a detailed view into an average plug was presented. In contrast to experimental setups were are not limited to measure the plug properties only at few locations. Experimental results usually provide the plug properties as a function of time at a given position along the tube, with the disadvantage that the plug profile is distorted by the relative motion of granulate along the plug. The vertical profiles were given for porosity, granular velocity, interparticle and drag forces, wall stress and granular temperature. In the experiment,

these parameters usually are not accessible along the whole tube.

Additionally the radial profile is given at high resolution. The results show that the grains are ordered in radial direction. The grains arrange themselves in layers along the tube wall. These layers have different velocities (up to 40% difference). Experimental measurements of the granular velocity using a CCD-Camera must take into account that they measure the velocity of the outer, slowest layer.

In conclusion, the model presented here is a useful tool for investigating plug conveying. It is fast and flexible enough to make parameter studies on full featured plug conveying and provides at the same time access to the plug properties at the level of grains. It can obtain both characteristic curves and plug profiles. Note also that the model can be easily used to describe horizontal transport, simply by rotating the gravitational acceleration. Future optimizations and faster computers will permit this model to be applied to industrial-sized systems.

## 6 Acknowledgments

We thank Ludvig Vinningland and Eirik Flekkøy for much help in the fluid solver, Thomas Ihle and Adriano de Oliveira Sousa for their general help and advice. This research was supported by DFG (German Research Community) contract HE 2732/2-1 and HE 2732/2-3.

## References

- [1] M. F. Al-Adel, D. A. Saville, and Sankaran Sundaresan. The effect of static electrification on gas-solid flows in vertical risers. *Industrial & Engineering Chemistry Research*, 41:6224–6234, Dec 2002.
- [2] S. Dasgupta, R. Jackson, and Sankaran Sundaresan. Gas-particle flow in vertical pipes with high mass loading of particles. *Powder Technology*, 96:6–23, Apr 1998.
- [3] A. Rautiainen, G. Stewart, V. Poikolainen, and P. Sarkomaa. An experimental study of vertical pneumatic conveying. *Powder Technology*, 104:139–150, Sep 1999.
- [4] T. Van den Moortel, E. Azario, R. Santini, and Lounès Tadrist. Experimental analysis of the gas-particle flow in circulating fluidized bed using a phase Doppler particle analyser. *Chemical Engineering Science*, 53:1883–1899, 1998.

- [5] David J. Mason and Avi Levy. A model for non-suspension gas-solids flow of fine powders in pipes. *International Journal of Multiphase Flow*, 27:415–435, 2001.
- [6] H. Biligen, E. Levy, and A. Yilmaz. Prediction of pneumatic conveying flow phenomena using commercial cfd software. *Powder Technology*, 95:37–41, Apr 1998.
- [7] Yasufumi Yamamoto, M. Potthoff, Toshitsugu Tanaka, T. Kajishima, and Yutaka Tsuji. Large-eddy simulation of turbulent gas-particle flow in a vertical channel: effect of considering inter-particle collisions. *J. Fluid Mech.*, 442:303–334, 2001.
- [8] David J. Mason and Avi Levy. A comparison of 1d and 3d models for the simulation of gas-solids transport systems. *Applied Mathematical Modelling*, 22:517–532, 1998.
- [9] Yutaka Tsuji, Toshitsugu Tanaka, and T. Ishida. Lagrangian numerical simulation of plug flow of cohesionless particles in a horizontal pipe. *Powder Technology*, 71:239–250, Aug 1992.
- [10] Y. Tomita and K. Tateishi. Pneumatic slug conveying in a horizontal pipeline. *Powder Technology*, 94:229–233, Dec 1997.
- [11] David J. Mason and J. Li. A novel experimental technique for the investigation of gas-solids flow in pipes. *Powder Technology*, 112:203–212, 2000.
- [12] K. W. Zhu, S. M. Rao, C. H. Wang, and S. Sundaresan. Electrical capacitance tomography measurements on vertical and inclined pneumatic conveying of granular solids. *Chemical Engineering Science*, 58:4225–4245, 2003.
- [13] N. Vasquez, L. Sanchez, G. E. Klinzing, and S. Dhodapkar. Friction measurement in dense phase plug flow analysis. *Powder Technology*, 137:167–183, Nov 15 2003.
- [14] E. Wassen and Th. Frank. Simulation of cluster formation in gas-solid flow induced by particle-particle collisions. *International Journal of Multiphase Flow*, 27:437–458, 2001.
- [15] W. Tsuji, Toshitsugu Tanaka, and Shigeru Yonemura. Cluster patterns in circulationg fluidized beds predicted by numerical simulation (discrete particle model versus two-fluid model). *Powder Technology*, 95:254–264, 1998.
- [16] Eivind Helland, René Occelli, and Lounès Tadrist. Numerical study of cluster formation in a gas particle circulating fluidized bed. *Powder Technology*, 95:210–221, 2000.
- [17] Kapil Agrawal, Peter N. Loezos, Madhava Syamlal, and Sankaran Sundaresan. The role of meso-scale structures in rapid gas-solid flows. *J. Fluid Mech.*, 445:151–185, 2001.
- [18] Yutaka Tsuji, Toshitsugu Tanaka, and Shigeru Yonemura. Particle induced turbulence. *Appl. Mech. Rev.*, 47:75–79, Jun 1994.

- [19] Toshitsugu Tanaka, Toshihiro Kawaguchi, Shota Nishi, and Yutaka Tsuji. Numerical simulation of two-dimensional fluidized bed: Effect of partition walls. *Fluids Engineering Division*, 166:17–22, Nov 1993.
- [20] Artur J. Jaworski and Tomasz Dyakowski. Application of electrical capacitance tomography for measurement of gas-solids flow characteristics in a pneumatic conveying system. *Meas. Sci. Technol.*, 12:1109–1119, 2001.
- [21] K. Konrad and T. S. Totah. Vertical pneumatic conveying or particle plugs. *The Canadian Journal of Chemical Engineering*, 67:245–252, Apr 1989.
- [22] W. Siegel. Grundlagen der pneumatischen Ppropfenförderung. In *Schüttgut I*, pages 95–101, 1995.
- [23] Gerhard Niederreiter and Karl Sommer. Modeling and experimental validation of pressure drop for pneumatic plug conveying. In *4th International Conference for Conveying and Particle Solids*, 2003.
- [24] Gerhard Niederreiter and Karl Sommer. Investigations on the formation and stability of plugs at dense-phase pneumatic conveying. In *World Congress on Particle Technology 4*, 2002.
- [25] M. Ye, M. A. van der Hoef, and J. A. M. Kuipers. A numerical study of fluidization behavior of Geldart A particles using a discrete particle model. *Powder Technology*, 139:129–139, Jan 2004.
- [26] Yutaka Tsuji, Toshihiro Kawaguchi, and Toshitsugu Tanaka. Discrete particle simulation of two-dimensional fluidized bed. *Powder Technology*, 77:79–87, Apr 1993.
- [27] Toshihiro Kawaguchi, Yasufumi Yamamoto, Toshitsugu Tanaka, and Yutaka Tsuji. Numerical simulation of a single rising bubble in a two-dimensional fluidized bed. In *International Conference on Multiphase Flow 1995*, pages 17–22, 1995.
- [28] Lu Huilin, He Yurong, and Dimitri Gidaspow. Hydrodynamic modelling of binary mixture in a gas bubbling fluidized bed using the kinetic theory of granular flow. *Chemical Engineering Science*, 58:1197–1205, 2003.
- [29] M. J. V. Goldschmidt, J. A. M. Kuipers, and W. P. M. van Swaaij. Hydrodynamic modelling of dense gas-fluidised beds using the kinetic theory of granular flow: effect of coefficient of restitution on bed dynamics. *Chemical Engineering Science*, 56:571–578, Jan 2001.
- [30] Shinichi Yuu, Toshihiko Umekage, and Yuuki Johno. Numerical simulation of air and particle motions in bubbling fluidized bed of small particles. *Powder Technology*, 110:158–168, 2000.
- [31] S. Limtrakul, A. Chalermwattanatai, K. Unggurawirote, Yutaka Tsuji, Toshihiro Kawaguchi, and W. Tanthapanichakoon. Discrete particle simulation of solids motion in a gas-solid fluidized bed. *Chemical Engineering Science*, 58:915–921, Mar 2003.

- [32] B. H. Xu and A. B. Yu. Numerical simulation of the gas-solid flow in a fluidized bed by combining discrete particle method with computational fluid dynamics. *Chemical Engineering Science*, 52:2785–2809, Aug 1997.
- [33] B. P. B. Hoomans, J. A. M. Kuipers, W. J. Briels, and W. P. M. van Swaaij. Discrete particle simulation of bubble and slug formation in a two-dimensional gas-fluidised bed: A hard-sphere approach. *Chemical Engineering Science*, 51:99–118, Jan 1996.
- [34] Shigeru Yonemura, Toshitsugu Tanaka, and Yutaka Tsuji. Cluster formation in gas-solid flow predicted by the dsmc method. *Gas-Solid Flows, ASME FED*, 166:303–309, 1993.
- [35] Avi Levy. Two-fluid approach for plug flow simulations in horizontal pneumatic conveying. *Powder Technology*, 112:46–272, 2000.
- [36] Kengo Ichiki and Hisao Hayakawa. Dynamical simulation of fluidized beds: Hydrodynamically interacting granular particles. *Phys. Rev. E*, 52:658–670, Jul 1995.
- [37] Sean McNamara, Eirik G. Flekkøy, and Knut Jørgen Måløy. Grains and gas flow: Molecular dynamics with hydrodynamic interaction. *Phys. Rev. E*, 61:4054–4059, Apr 2000.
- [38] H. P. G. D'Arcy. Les fontaines publiques de la ville de Dijon. *Victor Dalmont*, 1856.
- [39] P. C. Carman. Fluid flow through granular beds. *Trans. Inst. Chem. Engng.*, 26:150–166, 1937.
- [40] P. A. Cundall and O. D. L. Strack. Discrete numerical-model for granular assemblies. *Geotechnique*, 29:47–65, 1979.
- [41] Gerhard Niedereiter, Karl Sommer, Martin Strauß, Sean McNamara, and Hans J. Herrmann. in preparation.
- [42] J. Hong, Y. Shen, and Y. Tomita. Phase-diagrams in dense phase pneumatic transport. *Powder Technology*, 84:213–219, Sep 1995.